

Simultaneous phase and amplitude extraction from a single defocused image of a homogeneous object

D. PAGANIN^{*}†, S. C. MAYO*, T. E. GUREYEV*, P. R. MILLER* &
S. W. WILKINS*

*Commonwealth Scientific and Industrial Research Organization, Manufacturing Science and
Technology, PB 33 Clayton Stn, 3169 Victoria, Australia

†School of Physics, The University of Melbourne, 3010 Victoria, Australia

Key words. Holography, phase contrast, phase retrieval, point-projection microscopy, X-ray microscopy.

Summary

We demonstrate simultaneous phase and amplitude extraction from a single defocused image of a homogeneous object. Subject to the assumptions explicitly stated in the derivation, the algorithm solves the twin-image problem of in-line holography and is capable of analysing data obtained using X-ray microscopy, electron microscopy, neutron microscopy or visible-light microscopy, especially as they relate to defocus and point projection methods. Our simple, robust, non-iterative and computationally efficient method is applied to data obtained using an X-ray phase contrast ultramicroscope.

Introduction

Since the discovery of X-rays by Röntgen (1896), absorption has been the dominant principle of image formation in X-ray radiography (cf. Wilkins *et al.*, 1996; Pogany *et al.*, 1997; Gao *et al.*, 1998). As is well known, this mechanism of image formation often provides poor contrast when imaging light-element materials such as biological tissues.

Various schemes have been developed to combat such poor contrast. Within the dominant paradigm of absorption contrast, exploitation of the ‘water window’ in the wavelength range 2.3–4.3 nm (where water is almost an order of magnitude more transparent than organic material; Kirz *et al.*, 1995) has driven much research on the soft X-ray microscopy of biological structures (Sayre & Chapman, 1995; Jacobsen, 1999). At higher energies, however, phase provides a better contrast mechanism than absorption (Sayre & Chapman, 1995; Polack *et al.*, 1998) and allows one to image thicker

specimens (Kirz *et al.*, 1995; Sayre & Chapman, 1995). This motivated the use of various phase contrast methods in X-ray microscopy, such as Zernike-type phase contrast using annular phase plates in the back focal plane of a zone-plate lens (Schmahl *et al.*, 1994; Kirz *et al.*, 1995; Schneider *et al.*, 1998), interferometric phase contrast (Bonse *et al.*, 1998; Momose *et al.*, 1998), differential interference contrast (Kirz *et al.*, 1995; Polack *et al.*, 1998) and in-line holography (Kirz *et al.*, 1995; Sayre & Chapman, 1995; Lindaas *et al.*, 1998; Watanabe *et al.*, 1998).

An advantage of projection microscopy, using either X-rays or other forms of radiation, is its simplicity: no specialized optical elements are required in order to render phase shifts visible as intensity variations, because phase contrast may be achieved by the simple act of free-space propagation. This phenomenon is well known to optical microscopists, who use defocus to render transparent objects visible (see, e.g. Zernike, 1942). Under the name of ‘refraction contrast’, it is only recently that such propagation-induced phase contrast has been realized in X-ray imaging (White & Cerrina, 1992; Snigirev *et al.*, 1995; Cloetens *et al.*, 1996, 1997; Nugent *et al.*, 1996; Wilkins *et al.*, 1996). The absence of optical elements implies that such an imaging method is intrinsically free from the usual aberrations, with achievable resolution depending largely on the size of the source (Cosslett & Nixon, 1951; Pogany *et al.*, 1997). Another significant feature of the refraction-contrast method is its relaxed requirements on the temporal coherence of the radiation (Pogany *et al.*, 1997); indeed, the method has been demonstrated successfully using polychromatic radiation from a laboratory X-ray source (Wilkins *et al.*, 1996). Another advantage of using phase rather than absorption as the contrast mechanism is the reduced radiation dose imparted to the specimen (Schmahl *et al.*, 1994; Sayre & Chapman, 1995; Wilkins *et al.*, 1996).

Here we develop and apply a method for quantitative phase extraction using a single propagation-induced phase contrast

Correspondence: Dr D. Paganin, Australia. Tel. + 61 39545 2916; fax: + 61 39544 1128; e-mail: David.Paganin@csiro.au.

image taken using a point-projection microscope (the special case of plane-wave illumination is considered to be a limiting case). Subject to the assumptions explicitly stated in the derivation, the algorithm solves the twin-image problem of in-line holography and is capable of being used to analyse data obtained using point-projection X-ray microscopy, conventional transmission electron microscopy, point-projection electron microscopy, neutron microscopy or visible-light microscopy.

A summary of the remainder follows. We begin by introducing the ‘transport-of-intensity equation’ and use this as a starting-point to derive our algorithm for quantitative phase extraction from a single defocused image. We then describe a laboratory-based X-ray microscope used to experimentally demonstrate these ideas, and present propagation-induced phase contrast images of latex microspheres. Our new algorithm is then used to perform a quantitative single-image phase extraction on each phase contrast image. After a brief discussion, we offer some concluding remarks on some wider implications of the present approach.

Derivation of algorithm

We begin with the transport-of-intensity equation, which describes the intensity evolution of a paraxial monochromatic scalar electromagnetic or matter wave on propagation (Teague, 1983; Rytov *et al.*, 1989):

$$\nabla_{\perp} \cdot (I(\mathbf{r}_{\perp}, z) \nabla_{\perp} \phi(\mathbf{r}_{\perp}, z)) = -\frac{2\pi}{\lambda} \frac{\partial}{\partial z} I(\mathbf{r}_{\perp}, z). \quad (1)$$

Here, the intensity and phase of the beam are denoted by $I(\mathbf{r}_{\perp}, z)$ and $\phi(\mathbf{r}_{\perp}, z)$, respectively, λ is the radiation wavelength, the position vector \mathbf{r}_{\perp} lies in the plane perpendicular to the optic axis z , and ∇_{\perp} is the gradient operator in the plane containing \mathbf{r}_{\perp} .

A number of papers have used this equation to achieve quantitative non-interferometric phase imaging in the context of such diverse applications as adaptive optics (Roddier, 1990), visible-light microscopy (Barty *et al.*, 1998), electron microscopy (van Dyck & Coene, 1987; Bajt *et al.*, 2000; De Graef & Zhu, 2001), neutron microscopy (Allman *et al.*, 2000) and hard-X-ray imaging (Nugent *et al.*, 1996; Gureyev & Wilkins, 1998a,b; Gureyev *et al.*, 2000, 2001). For review articles on the subject, see Paganin & Nugent (2001) and Nugent *et al.* (2001). A common theme of this work is solution of the transport-of-intensity equation for the phase $\phi(\mathbf{r}_{\perp}, z)$, given non-interferometric measurements of the intensity $I(\mathbf{r}_{\perp}, z)$ and intensity derivative $\partial I(\mathbf{r}_{\perp}, z)/\partial z$.

To simplify the derivation of the algorithm for quantitative phase extraction from a single image, we first assume that the point-source of X-rays is at infinity (i.e. that $R_1 \rightarrow \infty$ in Fig. 1), leading to collimated illumination and unit magnification. At the end of the derivation, modifications due to finite R_1 are taken into account.

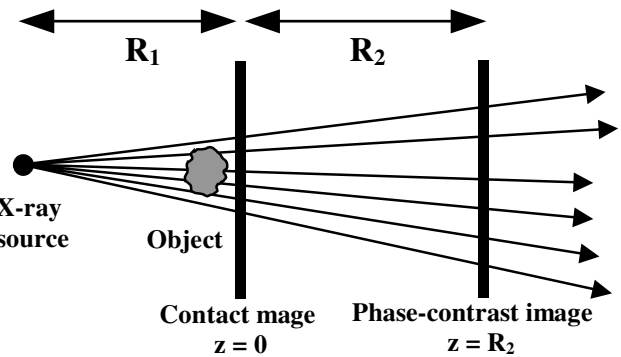


Fig. 1. Schematic for phase contrast imaging using a point source.

We assume that the object under study is composed of a single material, i.e. that the object is ‘homogeneous’. For normally incident plane-wave radiation of uniform intensity over the area occupied by the sample, the intensity of the radiation over the plane at the exit surface $z = 0$ ('contact image') of the object is assumed to be well approximated by Beer’s Law of absorption:

$$I(\mathbf{r}_{\perp}, z=0) = I^{in} e^{-\mu T(\mathbf{r}_{\perp})}. \quad (2)$$

Here, $T(\mathbf{r}_{\perp})$ is the projected thickness of the homogeneous object onto the plane over which the image is taken, μ is the linear attenuation coefficient, and I^{in} is the uniform intensity of the incident radiation. If the object is sufficiently thin, the phase $\phi(\mathbf{r}_{\perp}, z=0)$ of the illuminating beam at the exit surface of the homogeneous object is proportional to the projected thickness:

$$\phi(\mathbf{r}_{\perp}, z=0) = -\frac{2\pi}{\lambda} \delta T(\mathbf{r}_{\perp}), \quad (3)$$

where δ is the real part of the deviation of the material’s refractive index from unity (Wilkins *et al.*, 1996).

Substitute Eqs (2) and (3) into Eq. (1). The resulting equation is non-linear in $T(\mathbf{r}_{\perp})$, but it may be re-written as an equation linear in $\exp(-\mu T(\mathbf{r}_{\perp}))$:

$$-\frac{\delta}{\mu} I^{in} \nabla_{\perp}^2 e^{-\mu T(\mathbf{r}_{\perp})} = \frac{\partial}{\partial z} I(\mathbf{r}_{\perp}, z=0), \quad (4)$$

where use has been made of the identity

$$\delta \nabla_{\perp} \cdot (e^{-\mu T(\mathbf{r}_{\perp})} \nabla_{\perp} T(\mathbf{r}_{\perp})) = -\frac{\delta}{\mu} \nabla_{\perp}^2 e^{-\mu T(\mathbf{r}_{\perp})}. \quad (5)$$

Estimate the right-hand side of Eq. (4) using intensity measurements over two sufficiently closely spaced planes separated by a distance R_2 :

$$\frac{\partial}{\partial z} I(\mathbf{r}_{\perp}, z=0) \approx \frac{I(\mathbf{r}_{\perp}, z=R_2) - e^{-\mu T(\mathbf{r}_{\perp})} I^{in}}{R_2}. \quad (6)$$

Substitute Eq. (6) into Eq. (4) and re-arrange, to give

$$\left(-\frac{R_2 \delta}{\mu} \nabla_{\perp}^2 + 1 \right) e^{-\mu T(\mathbf{r}_{\perp})} = \frac{I(\mathbf{r}_{\perp}, z = R_2)}{I^{in}}. \quad (7)$$

To proceed further, represent both the contact image $I^{in} \exp(-\mu T(\mathbf{r}_{\perp})) = I(\mathbf{r}_{\perp}, z = 0)$ and the phase contrast image $I(\mathbf{r}_{\perp}, z = R_2)$ as Fourier integrals:

$$\begin{cases} I^{in} e^{-\mu T(\mathbf{r}_{\perp})} = \frac{I^{in}}{2\pi} \iint \mathcal{F}\{e^{-\mu T(\mathbf{r}_{\perp})}\} e^{i\mathbf{k}_{\perp} \cdot \mathbf{r}_{\perp}} d\mathbf{k}_{\perp} \\ I(\mathbf{r}_{\perp}, z = R_2) = \frac{1}{2\pi} \iint \mathcal{F}\{I(\mathbf{r}_{\perp}, z = R_2)\} e^{i\mathbf{k}_{\perp} \cdot \mathbf{r}_{\perp}} d\mathbf{k}_{\perp} \end{cases} \quad (8)$$

where $\mathcal{F}\{\}$ denotes Fourier transformation. Substitute into Eq. (7), to give

$$\mathcal{F}\{e^{-\mu T(\mathbf{r}_{\perp})}\} = \mu \frac{\mathcal{F}\{I(\mathbf{r}_{\perp}, z = R_2)\}/I^{in}}{R_2 \delta |\mathbf{k}_{\perp}|^2 + \mu}. \quad (9)$$

Taking the inverse Fourier transform (denoted \mathcal{F}^{-1}) of Eq. (9) and then solving for $T(\mathbf{r}_{\perp})$, we arrive at:

$$T(\mathbf{r}_{\perp}) = -\frac{1}{\mu} \log_e \left(\mathcal{F}^{-1} \left\{ \mu \frac{\mathcal{F}\{I(\mathbf{r}_{\perp}, z = R_2)\}/I^{in}}{R_2 \delta |\mathbf{k}_{\perp}|^2 + \mu} \right\} \right). \quad (10)$$

To conclude the derivation, we remove the assumption of an infinitely distant point source which was made at the start of this section. Using the Fresnel diffraction integral (see, e.g. Papoulis, 1981), one can show that the intensity $I_{R_1}(\mathbf{r}_{\perp}, z)$ downstream of a weakly refracting object illuminated by a point source at distance R_1 behind the said object, is related to the intensity $I_{\infty}(\mathbf{r}_{\perp}, z)$, which would result from normally incident collimated illumination of the same object, by (Pogany *et al.*, 1997):

$$I_{R_1}(\mathbf{r}_{\perp}, z) = \frac{1}{M^2} I_{\infty} \left(\frac{\mathbf{r}_{\perp}}{M}, \frac{z}{M} \right). \quad (11)$$

Here, $M = (R_1 + R_2)/R_1$ is the magnification of the image resulting from point-source illumination (see Fig. 1). Using Eq. (11), we transform Eq. (10) into a form suitable for point-source illumination:

$$T(\mathbf{r}_{\perp}) = -\frac{1}{\mu} \log_e \left(\mathcal{F}^{-1} \left\{ \mu \frac{\mathcal{F}\{M^2 I(M\mathbf{r}_{\perp}, z = R_2)\}/I^{in}}{R_2 \delta |\mathbf{k}_{\perp}|^2/M + \mu} \right\} \right). \quad (12)$$

Equation (12) is our final result. It shows how to solve the transport-of-intensity Eq. (1) for the projected thickness $T(\mathbf{r}_{\perp})$ of the homogeneous sample, using a single defocused image. Bearing Eqs (2) and (3) in mind, this projected thickness is trivially related to the intensity and phase of the radiation at the exit surface of the sample of interest.

By making use of the fast Fourier transform in the numerical implementation of Eq. (12), one has a rapid deterministic method for phase extraction from a single defocused image of a homogeneous object. One may think of the algorithm as an aberration-free virtual lens, which brings into focus the necessarily defocused images obtained using point-projection microscopy (Spence, 1992).

Experiment

Our basic set-up follows the principles of point-projection X-ray microscopy as described, for example, in the classic works of Cosslett & Nixon (1951, 1960). This approach may be traced back to von Ardenne's and Marton's independently conceived idea to generate a point source of X-rays by focusing electrons into a submicrometre spot on a suitable target (von Ardenne, 1939; Marton, 1939; Horn & Waltinger, 1978). More recent technical advances have included the use of a field-emission electron source and this appears to have first been proposed by Marton in 1951 (Newberry, 1995) and implemented by Kolaric & Svoboda (1989).

The essentials of the experimental set-up for the point-projection X-ray microscope used in the present studies are shown in Fig. 2, with further details available in Wilkins (1997). The microscope is based on a modified Hitachi S-450LB scanning electron microscope (SEM). A point source of X-rays was generated by focusing the 10 keV electron beam into a $\sim 0.25 \mu\text{m}$ spot on a tilted target consisting of a 300 nm layer of silver deposited on a silicon wafer substrate. This generated an X-ray spectrum, which was dominated by the characteristic $\text{AgL}\alpha$ lines at 3 keV. As shown in Fig. 2, the sample and CCD (charge coupled device) detector were mounted level with the target with the surface normal of the sample and detector at right angles to the vertical electron beam. The target-to-sample distance R_1 ranged from approximately 0.2–3.0 mm and the target-to-detector distance $R_1 + R_2$

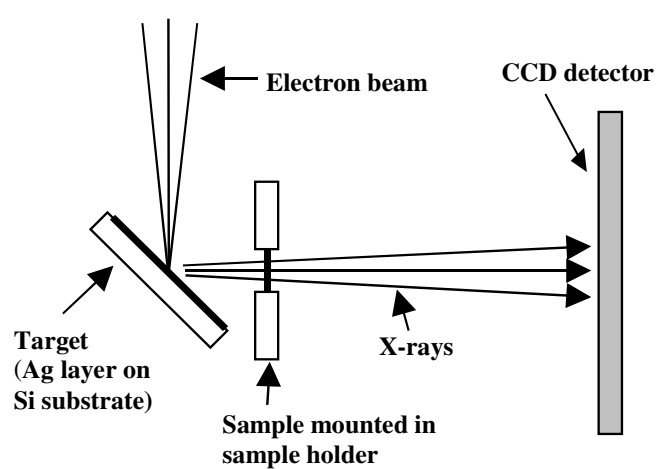


Fig. 2. Experimental set-up for phase contrast imaging using a point source.

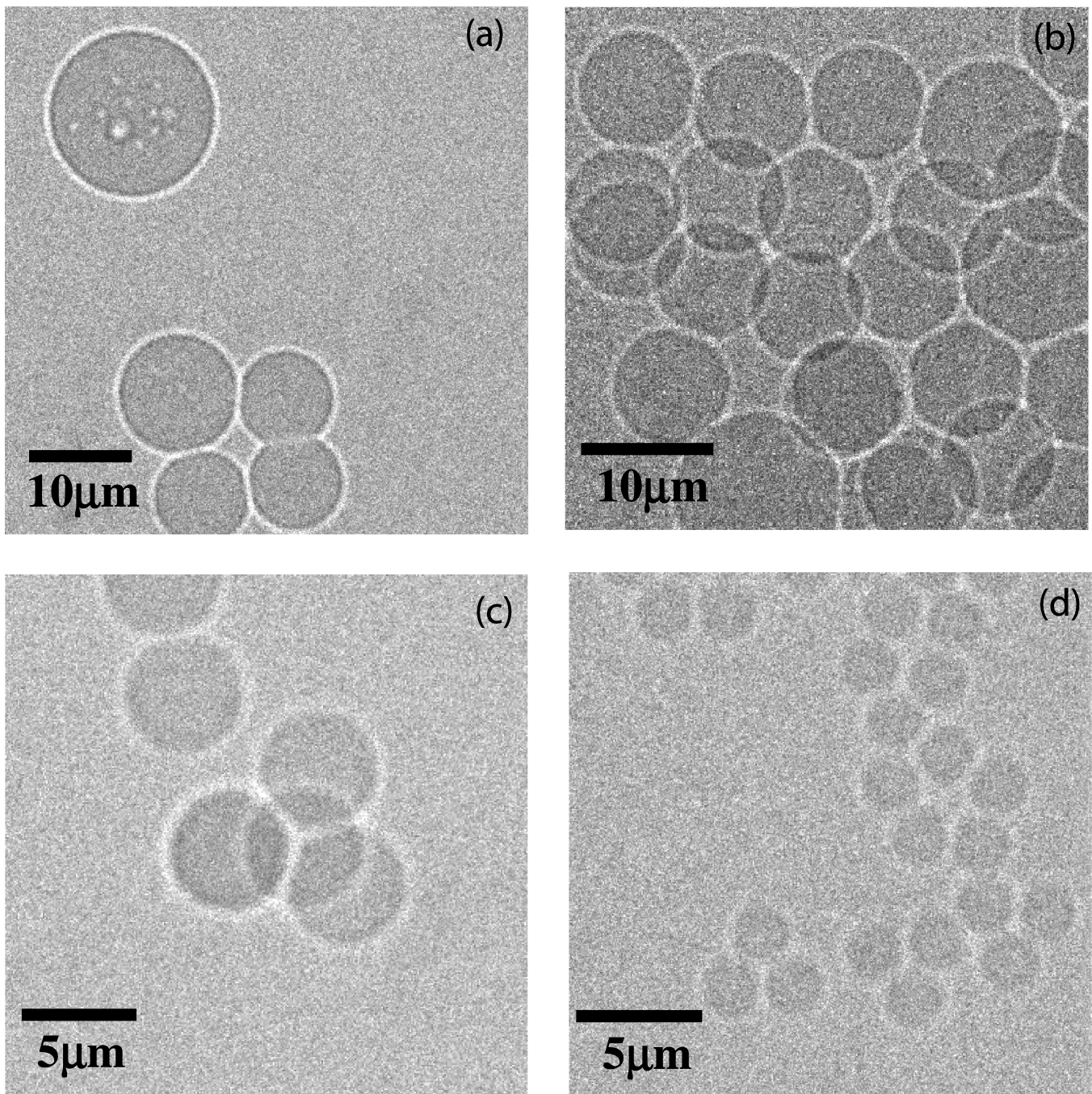


Fig. 3. Phase contrast X-ray images of latex spheres of varying size: (a) 9 μm ; (b) 9 μm ; (c) 5.2 μm ; (d) 2.3 μm . Exposure times were 25, 10, 35 and 25 min, respectively.

was 183 ± 2 mm. All images were collected using a 512×512 pixel Loral CCD array with 15 μm pixels. This was used in direct detection mode (i.e. without a phosphor screen) and was Peltier cooled to 232 K in order to minimize dark current generation during long exposures. A shutter was used to shield the CCD during readout.

As a well-characterized sample, we chose latex spheres of nominal diameters 2.3, 5.2 and 9 μm . At 3 keV, the linear

attenuation coefficient of latex is $\mu = 0.008276 \mu\text{m}^{-1}$ and the phase shift per unit length is $-0.4050 \text{ rad } \mu\text{m}^{-1}$. Four phase contrast images of these samples are shown in Fig. 3, at respective CCD-plane magnifications of 128 ± 3 , 187 ± 7 , 212 ± 6 , 248 ± 20 and with respective exposure times of 25, 10, 35, 25 min.

With reference to Fig. 3, the presence of significant propagation-induced phase contrast greatly increases the

visibility of the objects under investigation compared to what would be observed in contact mode. The dramatic edge-enhancement effect, which has been widely discussed in the literature (Zernike, 1942; White & Cerrina, 1992; Snigirev *et al.*, 1995; Wilkins *et al.*, 1996), is characteristic of propagation-induced phase contrast and serves in some sense to complement the absorption contrast evident in the image (see Pogany *et al.* (1997) for a precise formulation of this statement). Interestingly, the bubbles in the largest sphere of Fig. 3(a) act as lenses that weakly focus the beam, leading to an increase in intensity near the centre of these structures (cf. Fig. 3b in Wilkins *et al.*, 1996).

Analysis

The algorithm based on Eq. (12) was coded in the C++ language using a Fast Fourier Transform routine. We ascertained the correctness of the algorithm by successfully applying it to some simulated phase contrast images with similar parameters to those used in the experiment. The code was then used to analyse the four phase contrast images shown in Fig. 3. Each phase retrieval of a 512×512 pixel image took approximately 5 s on a Pentium-II 350 MHz personal computer. The results of the single-image thickness extraction are in Fig. 4.

It is important to verify the quantitative correctness of the extracted thickness profiles. (i) Fig. 4(c) contains a total of six spheres (ignoring the sphere which is 'cut off' at the top of the image, and counting two spheres at the location marked with an arrow). The maximum retrieved projected thickness of each of these six spheres averages to $4.8 \pm 0.6 \mu\text{m}$, which is consistent with the nominal value of $5.2 \mu\text{m}$. (ii) As a second test for the quantitative correctness of the retrieved images, we randomly chose 10 spheres from Fig. 4(d) and obtained the value $2.7 \pm 0.4 \mu\text{m}$ for the average maximum projected thickness of the spheres. This is consistent with the expected value of $2.3 \mu\text{m}$.

Discussion

With reference to Fig. 4, one notices the pleasing stability of the present algorithm with respect to significant amounts of noise in the input data. (i) The mathematical origin of this stability is due to the regularizing presence of a non-zero linear attenuation coefficient μ in Eq. (12), which avoids instability problems of the 'division by zero' type that would arise if μ were zero. (ii) The physical origin of this stability is readily explained in terms of the complementary nature of phase and absorption contrast in the small-defocus regime (Pogany *et al.*, 1997). We begin our physical explanation with the well-known fact that the weak absorption contrast of light-element samples renders their contact radiographs insensitive to fine structural details. Even so, absorption contrast is an excellent probe of detail at lower spatial frequencies. The situation is reversed for propagation-induced phase contrast, which is

more sensitive to higher-frequency phase structures in the object (such as edges), as they are more strongly diffracting than low-frequency structures. Phase structure at the lowest spatial frequencies gives a very weak phase contrast signal, leading to low-frequency instabilities in phase retrieved from such information. Because our algorithm uses both forms of contrast information simultaneously, it avoids low-frequency instabilities in the retrieved phase and is able to perform successfully even in the presence of large amounts of noise.

With its high degree of stability, one may think of the algorithm (12) as a practical aberration-free 'software lens', which brings into focus the necessarily defocused images obtained using point-projection microscopy (Spence, 1992). From another point of view, one may regard the algorithm as serving to decode the encrypted quantitative information present in a propagation-induced phase contrast image.

Looked at in this way, there are strong parallels with Gabor's original conception of in-line holography, which 'allows one to dispense altogether with ... objectives' and instead works with 'Micrographs [that] are obtained in a two-step process', namely, recording followed by reconstruction (Gabor, 1948). Indeed, the propagation-induced phase contrast images of Fig. 3 may be viewed as in-line holograms (Pogany *et al.*, 1997) for which the object-to-detector distance is sufficiently small for only a single Fresnel diffraction fringe to be significant. In light of this connection, we point out that the method for holographic reconstruction presented in this paper does not suffer from the well-known twin-image problem of in-line holography. Of course, the algorithm breaks down when applied to 'fully holographic' images containing multiple diffraction fringes, as the estimate on the right-hand side of Eq. (6) is then invalid. It is anticipated that a suitably generalized form of the present algorithm will be able to deal with such data.

We close this discussion with a brief look at the question of resolution. (i) Based on the images in Fig. 3, we estimate the source-size-induced blurring of our raw images to be consistent with object-plane convolution by a point spread function with a full width at half maximum of approximately $0.3 \mu\text{m}$. A decrease of such 'hardware blurring' is achievable (Wilkins, 1997). (ii) A second source of blurring, which we term 'software blurring', arises because the virtual lens of Eq. (12) relies on the approximation appearing on the right-hand side of Eq. (6). This approximation is only valid over length scales larger than $\sqrt{\lambda R_2/M}$, corresponding to a Fresnel number of unity (see Box 3 of Nugent *et al.*, 2001). Such 'aberrations' of our virtual lens could be corrected by the suitably generalized form of Eq. (12) mentioned at the end of the previous paragraph. (iii) There is an inherent limitation in the experimental set-up described here, where the source-to-detector distance was fixed. Because the resolution is limited by the source size, and as the field of view (referred to the object space) becomes smaller at higher magnification, the effective number of pixels (referred to the object space) also becomes very small at high magnification. This limitation does not apply to some of our

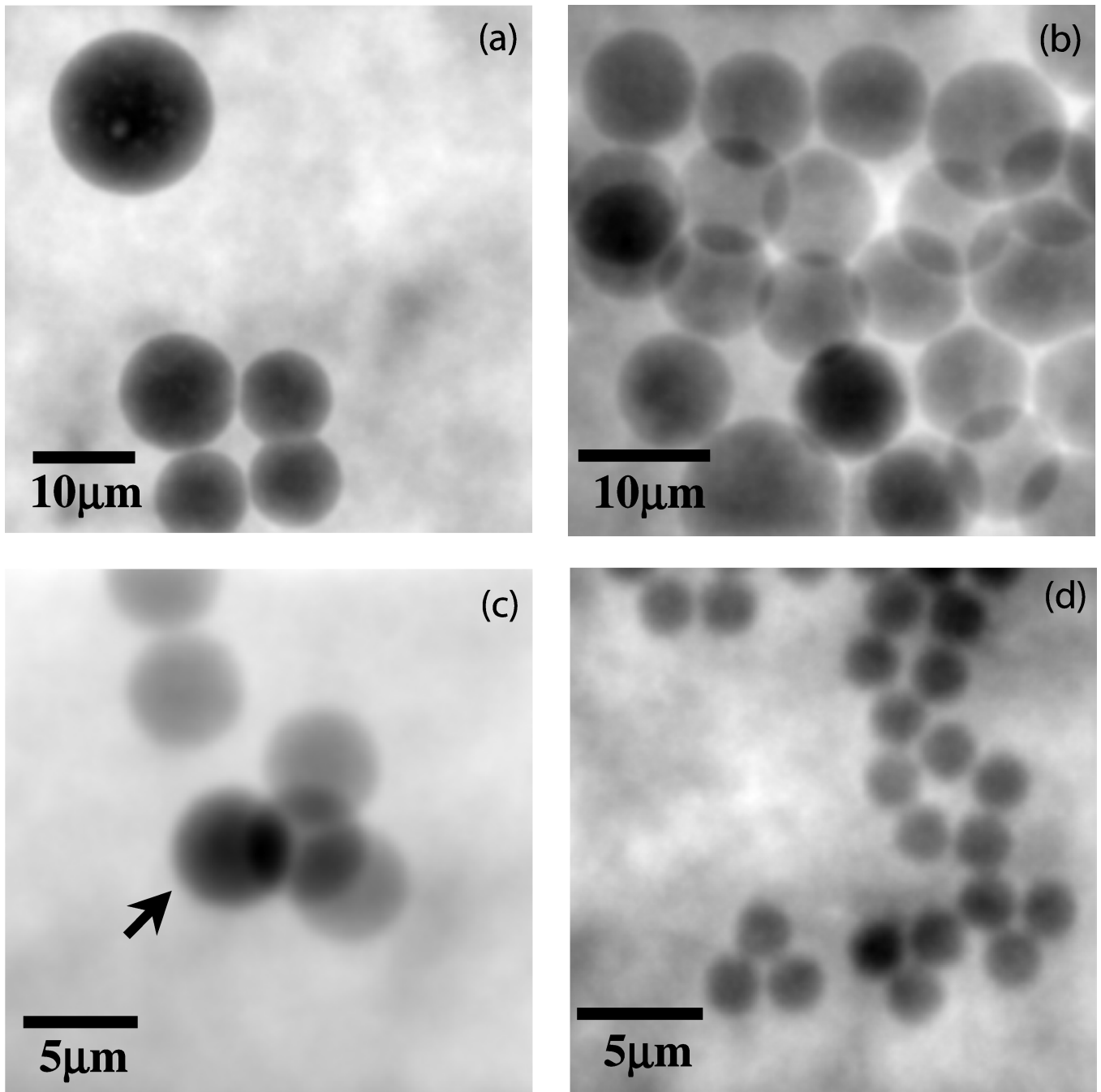


Fig. 4. Retrieved projected thickness as obtained from the X-ray phase contrast images in Fig. 3. Reverse contrast.

more recent experiments, which make use of a variable source-to-detector distance.

Conclusion

We developed a simple and practical algorithm for quantitative structure extraction from a single phase contrast image. This algorithm, which assumes that sufficiently

monochromatic radiation illuminates a homogeneous object, was successfully applied to data from a laboratory-based X-ray phase microscope. On account of its exceptional stability with respect to noise, computational speed and simplicity of implementation, we anticipate that this technique will find widespread use as a routine tool in medical, biological and industrial contexts that use hard X-rays, visible light, electrons or neutrons as a radiation probe.

Acknowledgements

The authors acknowledge the funding and support of X-ray Technologies Pty. Ltd. (XRT) for this research. D.P. acknowledges the support of an Australian Research Council SPIRT grant entitled *Robust analysis approaches for hard X-ray phase contrast imaging*. We are grateful to Andrew Stevenson for some help with the calculations. Thanks go to Andrew Pogany and Allan Morton for helpful comments, and to the anonymous referees for detailed and insightful reports.

References

- Allman, B.E., McMahon, P.J., Nugent, K.A., Paganin, D., Jacobson, D.L., Arif, M. & Werner, S.A. (2000) Quantitative phase radiography with neutrons. *Nature*, **408**, 158–159.
- von Ardenne, M. (1939) Zur Leistungsfähigkeit des Elektronen-Schattenmikroskopes und über ein Röntgenstrahlen-Schattenmikroskop. *Naturwissenschaften*, **27**, 485–486.
- Bajt, S., Barty, A., Nugent, K.A., McCartney, M., Wall, M. & Paganin, D. (2000) Quantitative phase-sensitive imaging in a transmission electron microscope. *Ultramicroscopy*, **83**, 67–73.
- Barty, A., Nugent, K.A., Paganin, D. & Roberts, A. (1998) Quantitative optical phase microscopy. *Opt. Lett.* **23**, 817–819.
- Bonse, U., Beckmann, F., Busch, F. & Günnewig, O. (1998) X-ray microtomography using interferometric phase contrast. *X-Ray Microscopy and Spectromicroscopy* (ed. by J. Thieme, G. Schmahl, D. Rudolph and E. Umbach), pp. I-77–I-83. Springer-Verlag, Berlin/Heidelberg.
- Cloetens, P., Barrett, R., Baruchel, J., Guigay, J.-P. & Schlenker, M. (1996) Phase objects in synchrotron radiation hard x-ray imaging. *J. Phys. D: Appl. Phys.* **29**, 133–146.
- Cloetens, P., Pateyron-Salomé, M., Buffière, J.-Y., Peix, G., Baruchel, J., Peyrin, F. & Schlenker, M. (1997) Observation of microstructure and damage in materials by phase sensitive radiography and tomography. *J. Appl. Phys.* **81**, 5878–5886.
- Cosslett, V.E. & Nixon, W.C. (1951) X-ray shadow microscope. *Nature*, **168**, 24–25.
- Cosslett, V.E. & Nixon, W.C. (1960) *X-Ray Microscopy*. Cambridge University Press, Cambridge.
- De Graef, M. & Zhu, Y. (2001) Quantitative noninterferometric Lorentz microscopy. *J. Appl. Phys.* **89**, 7177–7179.
- van Dyck, D. & Coene, W. (1987) A new procedure for wave function restoration in high resolution electron microscopy. *Optik*, **77**, 125–128.
- Gabor, D. (1948) A new microscopic principle. *Nature*, **161**, 777–778.
- Gao, D., Pogany, A., Stevenson, A.W. & Wilkins, S.W. (1998) Phase-contrast radiography. *Radiographics*, **18**, 1257–1267.
- Gureyev, T.E., Mayo, S., Wilkins, S.W., Paganin, D. & Stevenson, A.W. (2001) Quantitative in-line imaging with multi-energy X-rays. *Phys. Rev. Lett.* **86**, 5827–5830.
- Gureyev, T.E., Stevenson, A.W., Paganin, D., Mayo, S.C., Pogany, A., Gao, D. & Wilkins, S.W. (2000) Quantitative methods in phase-contrast X-ray imaging. *J. Digit. Imaging*, **13** (Suppl. 1), 121–126.
- Gureyev, T.E. & Wilkins, S.W. (1998a) On X-ray phase retrieval from polychromatic images. *Opt. Comm.* **147**, 229–232; Erratum. *Opt. Comm.* **154**, 391.
- Gureyev, T.E. & Wilkins, S.W. (1998b) On X-ray phase imaging with a point source. *J. Opt. Soc. Am. A*, **15**, 579–585.
- Horn, H.R.F. & Waltinger, H.G. (1978) How to obtain and use X-ray projection microscopy in the SEM. *Scanning*, **1**, 100–108 (1978).
- Jacobsen, C. (1999) Soft X-ray microscopy. *Trends Cell. Biol.* **9**, 44–47.
- Kirz, J., Jacobsen, C. & Howells, M. (1995) Soft X-ray microscopes and their biological applications. *Q. Rev. Biophys.* **28**, 33–130.
- Kolaříč, V. & Svoboda, V. (1989) An x-ray projection microscope with field emission gun. *J. Microsc.* **156**, 247–251.
- Lindaas, S., Calef, B., Downing, K., Howells, M., Magowan, C., Pinkas, D. & Jacobsen, C. (1998) X-ray holography of fast-frozen hydrated biological samples. *X-Ray Microscopy and Spectromicroscopy* (ed. by J. Thieme, G. Schmahl, D. Rudolph and E. Umbach), pp. II-75–II-86. Springer-Verlag, Heidelberg.
- Marton, L. (1939) Internal report, RCA Laboratories, Princeton.
- Momose, A., Takeda, T., Itai, Y. & Hirano, K. (1998) Phase-contrast X-ray microtomography: application to human cancerous tissues. *X-Ray Microscopy and Spectromicroscopy* (ed. by J. Thieme, G. Schmahl, D. Rudolph and E. Umbach), pp. II-207–II-211. Springer-Verlag, Heidelberg.
- Newberry, S.P. (1995) What happened to Marton's dream of a field emission X-ray microscope? *Zool. Studies*, **34** (Suppl. 1), 251–252.
- Nugent, K.A., Gureyev, T.E., Cookson, D., Paganin, D. & Barnea, Z. (1996) Quantitative phase imaging using hard X-rays. *Phys. Rev. Lett.* **77**, 2961–2964.
- Nugent, K.A., Paganin, D. & Gureyev, T.E. (2001) A phase odyssey. *Phys. Today*, **54**, 27–32.
- Paganin, D. & Nugent, K.A. (2001) Non-interferometric phase determination. *Advances in Imaging and Electron Physics* Vol. 118 (ed. by P. Hawkes), pp. 85–127. Academic Press, San Diego.
- Papoulis, A. (1981) *Systems and Transforms with Applications in Optics*. Krieger Publishing, Florida, p. 329.
- Pogany, A., Gao, D. & Wilkins, S.W. (1997) Contrast and resolution in imaging with a microfocus X-ray source. *Rev. Sci. Instrum.* **68**, 2774–2782.
- Polack, F., Joyeux, D. & Phalippou, D. (1998) Phase contrast experiments on the NSLS-X1A scanning microscope. *X-Ray Microscopy and Spectromicroscopy* (ed. by J. Thieme, G. Schmahl, D. Rudolph and E. Umbach), pp. I-106–I-109. Springer-Verlag, Heidelberg.
- Roddier, F. (1990) Wavefront sensing and the irradiance-transport equation. *Appl. Opt.* **29**, 1402–1403.
- Röntgen, W.C. (1896) On a new kind of rays. *Nature*, **53**, 274–276.
- Rytov, S.M., Kravtsov, Yu.A. & Tatarskii, V.I. (1989) *Principles of Statistical Radiophysics. Vol. 4: Wave Propagation Through Random Media*. Springer-Verlag, Berlin, p. 46.
- Sayre, D. & Chapman, H.N. (1995) X-ray microscopy. *Acta. Cryst. A* **51**, 237–252; Erratum. *Acta. Cryst. A* **51**, 810.
- Schmahl, G., Rudolph, D., Schneider, G., Guttman, P. & Niemann, B. (1994) Phase contrast X-ray microscopy studies. *Optik*, **97**, 181–182.
- Schneider, G., Schmahl, G., Schliebe, T., Peuker, M. & Guttman, P. (1998) Cryo X-ray microscopy in amplitude and phase contrast. *X-Ray Microscopy and Spectromicroscopy* (ed. by J. Thieme, G. Schmahl, D. Rudolph and E. Umbach), pp. I-111–I-115. Springer-Verlag, Heidelberg.
- Snigirev, A., Snigireva, I., Kohn, V., Kuznetsov, S. & Schelokov, I. (1995) On the possibilities of X-ray phase contrast microimaging by coherent high-energy synchrotron radiation. *Rev. Sci. Instrum.* **66**, 5486–5492.
- Spence, J.C.H. (1992) Convergent-beam nano-diffraction, in-line holography and coherent shadow imaging. *Optik*, **92**, 57–68.
- Teague, M.R. (1983) Deterministic phase retrieval: a Green's function solution. *J. Opt. Soc. Am. A*, **73**, 1434–1441.

- Watanabe, N., Sakurai, K., Takeuchi, A. & Aoki, S. (1998) Soft X-ray Gabor holography using CCD camera. *X-Ray Microscopy and Spectromicroscopy* (ed. by J. Thieme, G. Schmahl, D. Rudolph and E. Umbach), pp. II-291–II-295. Springer-Verlag, Heidelberg.
- White, V. & Cerrina, F. (1992) Metal-less X-ray phase shift masks for nanolithography. *J. Vac. Sci. Technol. B*, **10**, 3141–3144.
- Wilkins, S.W. (1997) High Resolution X-Ray Imaging of Very Small Objects. Australian Patent Application (PO 6041), PCT/AU98/00237.
- Wilkins, S.W., Gureyev, T.E., Gao, D., Pogany, A. & Stevenson, A.W. (1996) Phase-contrast imaging using polychromatic hard X-rays. *Nature*, **384**, 335–338.
- Zernike, F. (1942) Phase contrast, a new method for the microscopic observation of transparent objects. *Physica*, **9**, 686–693.